Journal of Medicinal Plants and By-Products (2025) 2: 137– 148

A Virtual Study on the Active Ingredients of *Zingiber officinale* and *Boswellia serrata* as Potential Natural Inhibitors of SARS-COV-2 Main Protease Enzyme

Mehr Ali Mahmood Janlou[1,2,*], Hassan Sahebjamee[3], Hamidreza Alaie[4] and Mahmoud Heidari[5]

[1]*Department of Biophysics, Faculty of Biological Sciences, Gorgan Branch, Islamic Azad University, Gorgan, Iran*
[2] *Medicinal Plants Research Center, Gorgan Branch, Islamic Azad University, Gorgan, Iran*
[3]*Department of Biophysics, Faculty of Biological Science, Varamin-Pishva Branch, Islamic Azad University, Varamin, I.R. Iran*
[4]*Department of Physics, Varamin-Pishva Branch, Islamic Azad University, Varamin, Iran*
[5]*Department of Biology, Faculty of Science, Gorgan Branch, Islamic Azad University, Gorgan, Iran*

Article Info

Article Type
Original Article

Article History
Received: 14 March 2024
Accepted: 27 August 2024

***Corresponding author**
mehr.janlou@gmail.com

ABSTRACT

SARS-CoV-2 is one of the most important novel coronaviruses and was recognized as a major global concern due to the declaration of the pandemic in March 2020. Researchers have attempted to develop antiviral agents against coronavirus, and the Mpro protein may be an effective drug target. To identify potential hit molecules for clinical use, we analyzed the inhibitory effects of phytochemical compounds from ginger and kundur and seven FDA-approved drugs against Mpro. Employing molecular docking and scoring functions, three top phytochemical compounds, gingerone A, astelbin, and L-(−)-catechin, and three reported antiviral drugs, chloroquine, ritonavir, and remdesivir, showed higher interaction profiles. According to the toxicity and ADME properties, L-(−)-catechin and remdesivir were selected for further analysis via MD simulations. The MD results supported by standard analysis (e.g., RMSD, RMSF, Rg, and SASA) revealed that L-(−)-catechin had a greater impact on the Mpro structure than remdesivir. Proteinligand energy calculations via the MM/PBSA method also supported the molecular docking data. Interestingly, our docking studies revealed that L-(−)-catechin has different interactions with Cys145 and His41, which may disrupt the formation of the Cys-His dyad, which is crucial for Mpro protease activity. We believe that due to the significant effect of L-(−)-catechin on the Mpro protein, this compound can be evaluated as a candidate molecule in drug development studies against SARS-CoV-2.

Keywords: SARS-COV-2 main protease, Kundur, Ginger, Docking, MD simulation

How to cite this paper
Mahmood Janlou, M.A., Sahebjamee, H., Alaie, H., Heidari, M. A Virtual Study on the Active Ingredients of *Zingiber officinale* and *Boswellia serrata* as Potential Natural Inhibitors of SARS-COV-2 Main Protease Enzyme. Journal of Medicinal plants and By-Products, 2025; 14(2): 137-148. doi: 10.22034/jmpb.2024.365268.1670

INTRODUCTION

SARS-CoV-2 belongs to the subfamily Coronavirinae and is a member of the Coronaviridae family that can cause an array of diseases ranging from mild cold-like illnesses to lethal respiratory tract infections in humans [1]. The catastrophic outbreak of SARS-CoV-2 in 2019 resulted in 561 million confirmed cases of COVID-19, causing >7 million deaths worldwide by 7 January 2024, according to the World Health Organization (WHO) (https://covid19.who.int/). Although this has led to the production of vaccines by pharmaceutical companies such as Pfizer/BioNTech, Moderna, AstraZeneca, and emergency use in countries after demonstrating efficacy in clinical trials [2], the virus generation is not extinct, and more or less deaths continue. As the coronavirus continues to evolve, new variants are emerging in which a few mutations make the virus more infectious or even deadly. In the last 20 years, the generation and emergence of three respiratory coronaviruses from mammalian reservoirs into human populations, have suggested that the next coronaviruses will be generated and emerge. Using computer analysis, three University of Liverpool researchers demonstrated that coronaviruses undergoing frequent host-shifting events between nonhuman animals and humans or nonhuman animal species, carry out a natural process of homologous recombination, which brings together new combinations of genetic material, and hence new viral strains, from two similar nonidentical parent strains of the virus [3]. It is possible that coronaviruses, due to certain types of mutations, may become resistant to vaccines and spread again worldwide. Therefore, finding new treatment strategies for, effective and affordable treatment of this dangerous infection is vital.

SARS-CoV-2 is a single-stranded positive-sense RNA virus that encodes two polyproteins (PP1a and PP1ab). After the entry of SARS-CoV-2 into host cells, enzymes such as serine protease, cysteine protease, papain-like protease, and the main protease (Mpro) are involved in the replication and life cycle of the virus through the cleavage of viral polyproteins [4]. Unlike other viral proteolytic enzymes, SARS-CoV-2 Mpro has no close

homologous with human proteases or the consequent drawbacks of nonspecific inhibition. However, it is widely conserved among members of the same family, such as MERS-CoV and SARS-CoV Mpro [5]. This has made it an important drug target for researchers to inhibit virus replication [6-8]. Structurally, Mpro is a homodimeric protease. Each protomer contains three domains, I, II, and III. The binding pocket of SARS-CoV-2 Mpro includes approximately 9 polar (Cys145, Ser144, Asp187, His163, His164, His41, Glu166, Gln189, and Asn142) and 5 nonpolar (Gly143, Phe140, Met165, Met49, and Thr26) key residues. Among them, Cys145 and His41 constitute a conserved catalytic dyad located between domains I and II [9]. His41 provides the optimal pH for nucleophilic attack of the cysteine-SH group for substrate hydrolysis [10]. They cleave polyproteins by proteolytic action to form nonstructural polypeptides. These polypeptides are needed to generate four necessary structural proteins (spike-RBD, membrane, nucleocapsid, and envelope proteins) and other subordinate proteins [11].

The best approach to combat the possible new epidemic caused by SARS-CoV-2 could be the development of safe and selective drugs. Despite many efforts by researchers, no potentially active drugs that can effectively combat SARS-CoV-2 have been reported to date. Repurposing FDA-approved drugs, such as remdesivir, favipiravir, chloroquine, hydroxychloroquine, indinavir, lopinavir, and ritonavir, have shown potential for the treatment of severe acute respiratory syndrome 2 (SARS-CoV-2). However, not only have many adverse effects been reported, such as lopinavir, which eliminated the symptoms of COVID-19 in early clinical trials but also, there are no effective clinically approved drugs available for treating this disease [12-15]. Clinical studies revealed that the use of repurposing drugs has no real impact on COVID-19 infection and is often futile in patients with severe symptoms [10].

One notable approach relies on the use of potential phytochemical compounds whose pharmacological profile for the treatment of COVID-19 suggests that they may be beneficial for patients. The present study aimed to determine the potential compounds that target SARS-CoV-2 Mpro and how to inhibit Mpro from natural sources such as *Zingiber officinale* Roscoe and *Boswellia serrata* Roxb. The use of herbal medicines to treat many diseases has been customary in many countries, such as India, China, and Iran, since ancient times. Even today, due to its advantages, such as inexpensiveness, effectiveness with few side effects, ability to cater to a growing population, and accuracy in mentioning the healing power of various plants, it still persists [16]. In some East Asian countries, such as India, one of the traditional Hindu systems of medicine is called Ayurveda. Among the large number of plants that are part of Ayurvedic medicine in India and Bangladesh, Kundur and Ginger are the most important medicinal plants; therefore, these plants are often referred to as "Mahaushadha" and "Vishvabhesaja", respectively, to determine their special status [17,18]. Kundur gum resin extract has been proven to have a wide range of anti-inflammatory effects, such as against arthritis, diabetes, asthma, cancer, and inflammation, due to the presence of various bioactive compounds, including mono-, di-, and triterpenes-, and sterols, etc., [19-21]. In addition, compounds in ginger are known to be effective against various viruses [22]. The lyophilized juice extract of ginger is considered to have antiviral effects on hepatitis C virus infection. In a particular study, ginger was proven to be effective at inhibiting viral replication inside hepatitis C virus-infected Hep G2 cells by affecting viral RNA [23].

In the present investigation, we selected 13 natural compounds, Ginger and Kundur, and evaluated their inhibitory potency against SARS-CoV-2 Mpro. To determine the binding affinities and interactions of the selected molecules, computational techniques such as molecular docking were performed. In addition, additional validation techniques, such as molecular dynamics (MD) simulations, were used following the MM-PBSA analysis of the top compounds identified through analysis of docking simulations to confirm the proposed candidate interactions and binding affinity. The interactions of the best-scoring ligands in this study were investigated in depth. We hope that the knowledge gained in this investigation will result in progress in clinical studies and treatment of SARS-CoV-2 infections.

MATERIALS AND METHODS

Plant Phytochemical Retrieval and Preparation

The structures of 13 active compounds present in Ginger and Kundur [18, 24, 25], the experimental cocrystallized ligand, and 7 FDA-approved drugs repurposed for the treatment of COVID-19 during 2020 were downloaded from the ChemSpider and DrugBank databases, respectively, in mol format. An open Babel molecule format converter [26] was used for the conversion of 2D to 3D conformations and the conversion of .mol to .mol2 files. For minimalenergy molecular geometries, all mol2 files were optimized using HyperChem 7.5 with the B3LYP/6-31G* type of basis set. Fig. 1 shows the 2D structures of these active and potential compounds.

Preparation of Mpro

The 3D structure of the SARS-CoV-2 main protease (PDB ID: 5RFS) was taken from the RCSB PDB (http://www.rcsb.org). The resolution of the retrieved structure was 1.70 Å. The crystal structure of the main protease was loaded into UCSF Chimera (https://www.cgl.ucsf.edu/chimera/) for molecular docking preparation [27]. The protein structure was

refined by removing the ligand, heteroatoms, and water. Water molecules are usually removed by semi-flexible and rigid docking because the formation of receptorligand complexes might be affected by fixed water molecules. Furthermore, the Gasteiger charges and hydrogen atoms were added. Finally, the drug targets were saved in PDB format with their respective PDB IDs for docking studies.

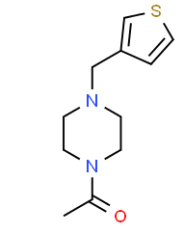

1: Co-cristallized ligand

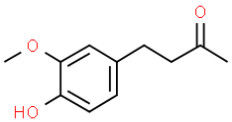

2: Zingerone

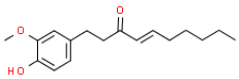

3: Shogaol

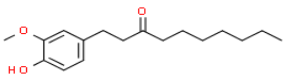

4: Paradol

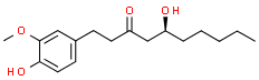

5: Gingerol

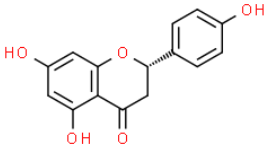

6: Naringenin

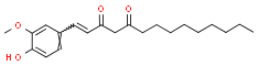

7: 1-dehydro

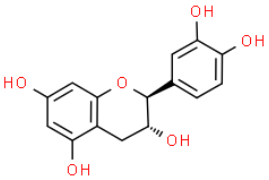

8: L-(−)-Catechin

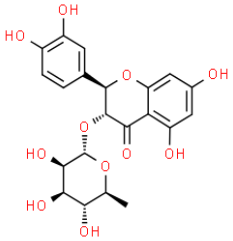

9: Astilbin

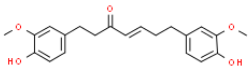

10: Gingerenone A

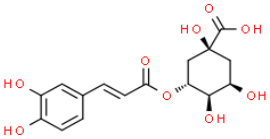

11: Chlorogenic acid

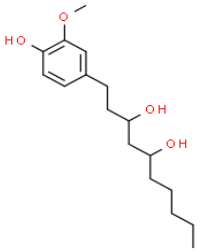

12: Gingerdiol

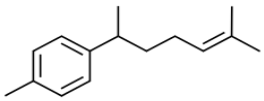

13: Curcumene

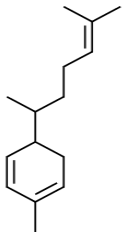

14: Zingiberene

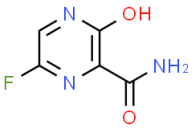

15: Favipiravir

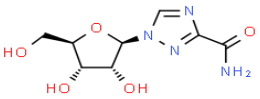

16: Ribavirin

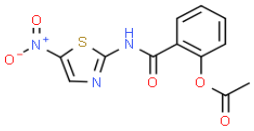

17: Nitazoxanide

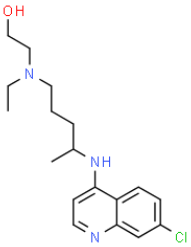

18: Hydroxychloroquine

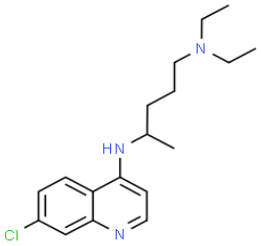

19: Chloroquine

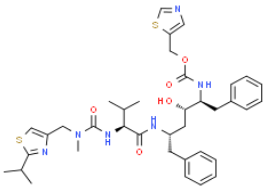

20: Ritonavir

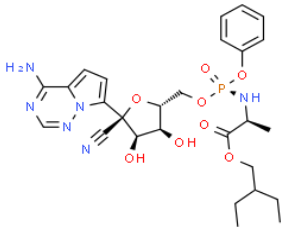

21: Remdesivir

Fig. 1 2D structure of 13 active ingredients, co-crystallized ligand, and 7 potential drugs.

Molecular Docking

Using the binding method, the ability to estimate the scoring function and evaluate the proteinligand interaction can be used to predict the binding affinity. AutoDock 4.2 software [28] was used to determine the bioactive binding affinities of the ligands in the binding pocket of COVID-19 Mpro. The crystal structure of 5RFS was used to define the binding site of Mpro. The binding site was defined after removing the cocrystallized ligand, and the grid was generated using the following grid box's center points: X: -1.333, Y: -2.917, and Z: 18.250. The spacing between grid points was kept at 0.375 Å, and the number of points in the X, Y, and Z dimensions was 46, 40, and 38, respectively, with a suitable grid box volume where each of the ligands can easily be fitted and which covers the entire active site pocket. During docking, the receptor is rigid, while the ligands are flexible. To explore the configuration spaces available for the interaction between the ligand and receptor, the genetic algorithm (GA) method was used. It is a stochastic search algorithm for computational optimization inspired by the principles of natural selection and genetics. For each independent run, the number of genetic algorithm runs was set to 100. The other parameters were set to their defaults in the AutoDock software. For all reference and target ligands, the same grid box size and other parameters were used. The Lamarckian genetic algorithm was used for the molecular docking process and to find the best conformers. The dock results were saved for the observation of binding affinities. Additionally, 2D and 3D binding interactions between ligands and targets were analyzed by Discovery Studio Client 2017 and PyMol software, respectively.

Drug-likeness and ADMET Properties Assessment

The drug-likeness, pharmacokinetic properties, and toxicity of potential lead compounds are very important for reducing side effects in the pharmaceutical industry. In this study, two web-based SwissADME (http://www.swissadme.ch/) and ProTox-II (http://tox.charite.de/protox_II) algorithms were used to determine the drug-likeness and ADMET properties of the compounds that had the best binding affinity for the Mpro protein. The mol format of each compound was used as an input file for these web servers.

Molecular Dynamics Simulation and MM/PBSA Analysis

The dynamics of the interactions between the mentioned protein and ligand(s) were then investigated using molecular dynamics (MD) simulations as follows: Simulations were performed using GROMACS version 5.1.1. [29-31].

Protein parameters were generated using the gromos53a6 force field. Ligand parameters for the same force field were generated using the PRODRG server [32]. The Gmx editconf tool was used to generate a dodecahedron simulation box. Solvation was performed with the SPC water model using the gmx solvate tool. The net charge of the Mpro protein was -4, so neutralization of the system required the addition of 4 Na+ ions. The entire system was minimized using the steepest descent of 1000 steps followed by conjugate gradients of 50000 steps. After energy minimization, the system was equilibrated in two steps: In the first step of 1000 picoseconds of NVT equilibration, the system was heated to 300 K to stabilize the temperature of the system. In the second step, 1000 picoseconds of the NPT ensemble, bond lengths were constrained in their equilibrium values using the linear constraint solver (LINCS) algorithm [30]. Long-range interactions were handled using the particle mesh Ewald (PME) summation method [33]. In the final step of the MD simulation, equilibrium geometries were achieved using an MD simulation for 100ns100 ns at 300 K with a step time of 2 fs. The root mean squared deviation (RMSD) and root mean squared fluctuation (RMSF) of the proteins were computed using the gmx rmsd and gmx rmsf tools, respectively. The solvent accessible surface area (SASA) and radius of gyration (Rg) were also measured by the gmx sasa and gmx gyrate tools, respectively. The strength of the protein-ligand interaction energies in a dynamic state was estimated with molecular mechanics Poisson–Boltzmann surface area (MM/PBSA) binding free energy calculations by utilizing the g_mmpbsa script of GROMACS [34]. The coulombic short-range (SR), Lennard–Jones interactions, polar and nonpolar solvation energies were computed between the target protein and ligand to determine complex stability.

Free energy landscape (FEL)

Principal component analysis (PCA) is used as a standard tool in statistical mechanics to determine the correlated motions of the residues to a set of linearly uncorrelated variables called principal components. In this study, the Cα atoms of target proteins were selected for the estimation of fluctuations, which are important characteristics of essential internal motions. The results obtained from PCA were subjected to free energy landscape (FEL) assessment, to determine the probability energy distribution of one or more collective variables of the protein system along with the Gibbs free energy, which helps to visualize the stability of different conformations of a protein [35]. 2D representations of the FEL from the trajectory were extracted using gmx_sham in GROMACS [30].

RESULTS AND DISCUSSION

Molecular Docking Analysis

This method has been widely used to predict the potential inhibitory effects of compounds and repurpose drugs against various target proteins. Table 1 shows the binding affinities of several well-known potentially active drugs against SARS-CoV-2 Mpro. The docking resutls show that the top three phytochemicals (Chloroquine, Ritonavir, and Remdesivir) demonstrated binding energy between -7.23 and -7.56 kcal/mol. Accordingly, it seems reasonable that the cutoff binding energy to filter the active ingredients to be <-8kcal/mol. The docking process of phytochemicals and cocrystallized ligand onto the active site of Mpro revealed that three compounds, Gingerenone A, Astilbin, and L-(−)-catechin, have better binding potential than the other compounds (Table 2). The binding energy score was used for assessing the strength of proteinligand interactions and ranking them accordingly. A more negative binding energy score suggested more favorable binding between the ligand and protein. The Discovery Studio visualizer was used to examine the residues that interact between the active site and the molecules. The interactions of the experimental co-crystalized ligand (5RFS), a reported antiviral with a binding energy <-7 kcal/mol (i.e., chloroquine, ritonavir, and remdesivir), and the top three phytochemicals, gingerenone A, astilbin, and L-(−)-catechin, with Mpro were explored in-depth by analyzing their binding patterns. Examination of the binding poses revealed that all the docked compounds interacted with the Mpro binding site, thereby revealing their potential inhibitory effects on the Mpro of SARS-CoV-2. A comparison of the docked poses of these molecules and the co-crystallized ligand showed a similar interaction pattern. In both the docked complexes and the experimental cocrystal structure, the molecules interacted with the same residues (Gly143, Cys145, His41, Ser144, Met49, Phe140, Glu166, Asn142, Gln189, and Met165) and other critical residues essential for inhibition, as shown in Fig. 2. The formation of a similar binding pattern confirmed that the docking simulation study was reliable for reproducing the experimental binding mode of SARS-CoV-2 Mpro. In the binding pose of the docked structures, there are hydrogen bond interactions. In addition, dominant electrostatic interactions and vdW interactions are also present. In particular, our docking studies showed that the selected ligands, such as experimental co-crystallized ligand, have various interactions with Cys145 and His41, which may disrupt the formation of the Cys-His dyad, which is crucial for Mpro protease activity. In Table 3, the binding interactions of the top three phytochemicals, the co-crystallized ligand chloroquine, ritonavir, and remdesivir, against the active site of the Mpro enzyme are summarized.

Drug-likeness and ADMET Properties

Druglikeness and ADMET (absorption, distribution, metabolism, excretion, and toxicity) properties are important criteria that are considered during the drug development process and are the main filtration steps for the drug design process [36, 37]. Therefore, from an economic point of view, tracking these issues in the early stages can be beneficial. Given these findings, the three best compounds, viz., Astilbin, L-(−)-catechin, and gingerenone A, which have binding energies ≤8 kcal/mol, as well as chloroquine, ritonavir, and remdesivir, which are potential drugs with binding energies <-7 kcal/mol, were subjected to various toxicity and ADME modules. The toxicity predicted by protox-II is listed in Table 4. The organ and endpoint toxicity (hepatotoxicity, carcinogenicity, immunotoxicity, mutagenicity, and cytotoxicity) predictions depicted inactive scores for three compounds, L-(−)-catechin, gingerenone A, and remdesivir. Among these, the predicted LD50 of L-(−)-catechin was greater than that of the other inhibitors.

The prediction of pharmacokinetic properties among the three selected phytochemical compounds revealed that only L-(−)-catechin was not only efficiently absorbed by the gastrointestinal tract, which had a low blood-brain barrier (BBB) permeability value, but also did not affect on the cytochromes CYP1A2, CYP2C19, CYP2D6, CYP2C9, and CYP3A4. Additionally, the prediction results revealed that L-(−)-catechin has no violation of the drug-likeness properties of Lipinski's rule of five. On the other hand, among the three selected potential approved drugs, remdesivir has better conditions in terms of toxicity and ADME properties. First, it has a lower toxicity than chloroquine and ritonavir. Second, the BBB is predicted to not penetrate the CNS, a P-gp substrate (and hence actively pumped from the brain to the gastrointestinal lumen) or an inhibitor of most cytochromes (CYP1A2, CYP2C19, CYP2C9, and CYP2D6) (Table 5). Overall, from the binding affinity, toxicity level, and ADME analysis, we selected the docked complex of remdesivir (as a reference) and the hit phytochemical L-(-)-catechin to further analyze the binding free energy and stability of these molecules by molecular dynamic simulation and MM/PBSA. Although the WHO has cautioned against the excessive use of remdesivir since November 2020, it was nevertheless considered the best candidate for treating COVID-19 in the U.S. [38]. This drug has been authorized for temporary use as a treatment for COVID-19 in many countries around the world [39].

Comparative effectiveness studies have shown that remdesivir induces rapid clinical improvement. Studies have indicated that remdesivir is active against viral strains, especially retroviruses, and potentially inhibits their replication; thus, remdesivir can be considered a reference for the development of a new anti-coronavirus agent [40].

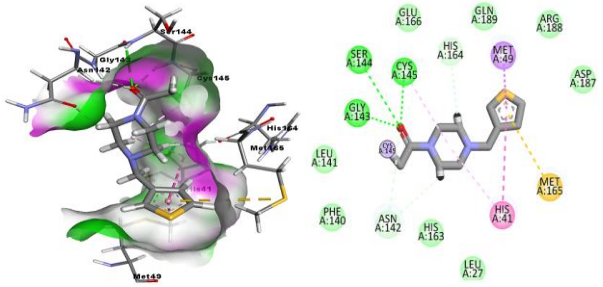

Co-crystalized ligand

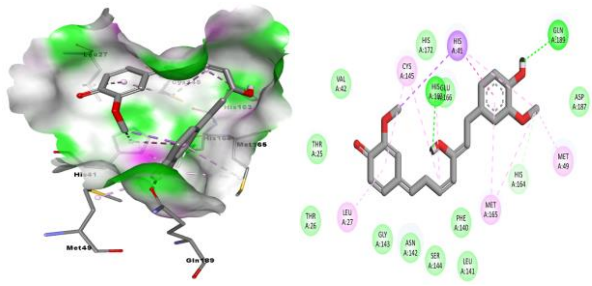

Gingerenone A

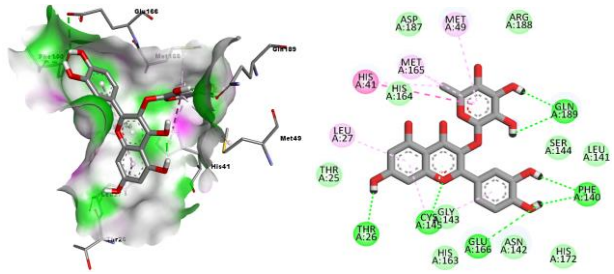

Astilbin

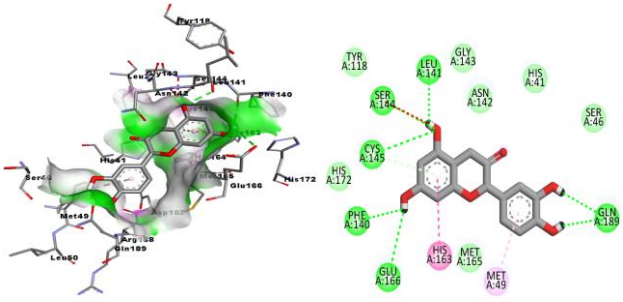

L-(−)-Catechin

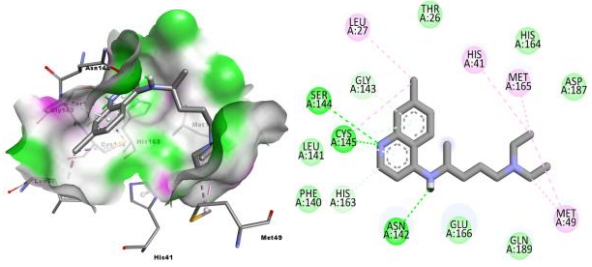

Chloroquine

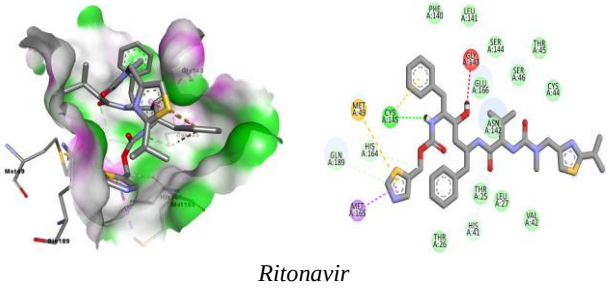

Ritonavir

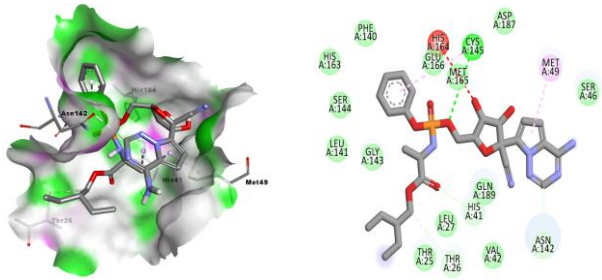

Remdesivir

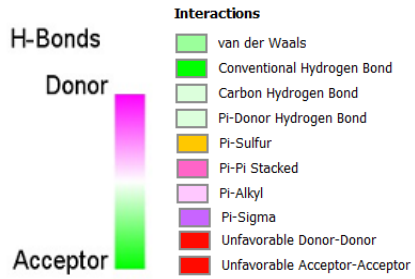

Fig. 2 Pose view and receptor-ligand interactions of the Co-crystallized ligand, top three reported antiviral, and phytochemicals.

Results of the Molecular Dynamics Analysis

Since molecular docking provides static entities from proteinligand interactions, MD simulation can be an important part of any computational analysis. Also, It supplements detailed data concerning proteinligand interactions with a dynamic aspect [41]. To obtain more profound insights into the impact of conformational flexibility and structural alterations on the interaction profiles of the complexes, we allowed unbound-(Apo) Mpro and two selected Mpro–ligand complexes to undergo MD simulations at the 100 ns scale. RMSD, RMSF, Rg, SASA, the number of H-bonds in the complexes, and eventually the MM/PBSA-based total binding free energy of the selected ligands were determined by MD simulations through the GROMACS approach. The RMSD between the backbone of the protein atoms relative to the initial conformation for Apo and bound Mpros was calculated to determine the stability of the system and quantify the degree of conformational change. The results of this study revealed a stable system for Apo-Mpro throughout the trajectory

(Fig. 3(a)). On the other hand, an increase in the RMSD values of the docked structures throughout the simulation suggested protein instability after ligand binding.

Table 1 Binding energies of some FDA-approved drugs repurposed for the treatment of COVID-19 during 2020 against Mpro.

No	Inhibitors	MF	MW (Da)	Binding energy (kcal/mol)
1	Favipiravir	$C_5H_4FN_3O_2$	157.103	-4.24
2	Ribavirin	$C_8H_{12}N_4O_5$	244.205	-5.25
3	Nitazoxanide	$C_{12}H_9N_3O_5S$	307.282	-6.74
4	Hydroxychloroquine	$C_{18}H_{26}ClN_3O$	335.871	-6.88
5	Chloroquine	$C_{18}H_{26}ClN_3$	319.872	-7.23
6	Ritonavir	$C_{37}H_{48}N_6O_5S_2$	720.944	-7.34
7	Remdesivir	$C_{27}H_{35}N_6O_8P$	602.576	-7.56

Table 2 Binding energies of active ingredients and Co-crystallized ligand against Mpro.

No	Inhibitors	MF	MW (Da)	Binding energy (kcal/mol)
1	Zingerone	$C_{11}H_{14}O_3$	194.227	-5.89
2	Gingerdiol	$C_{17}H_{28}O_4$	296.402	-5.95
3	Chlorogenic acid	$C_{16}H_{18}O_9$	354.309	-6.27
4	Curcumen	$C_{15}H_{22}$	202.335	-6.5
5	Co-crystallized ligand	C11H16N2OS	224.32	-6.54
6	Zingiberene	$C_{15}H_{24}$	204.351	-7.04
7	Shogaol	$C_{17}H_{24}O_3$	276.371	-7.05
8	Paradol	$C_{17}H_{26}O_3$	278.387	-7.12
9	Gingerol	$C_{17}H_{26}O_4$	294.386	-7.13
10	Naringenin	$C_{15}H_{12}O_5$	272.253	-7.21
11	1-dehydro-10-Gingerdione	$C_{21}H_{30}O_4$	346.461	-7.44
12	L-(−)-Catechin	$C_{15}H_{14}O_6$	290.268	-8.07
13	Gingerenone A	$C_{21}H_{24}O_5$	356.412	-8.36
14	Astilbin	$C_{21}H_{22}O_{11}$	450.393	-8.56

Table 3 Binding Interactions of the cocrystallized ligand, top three reported antiviral, and phytochemicals, against the active site of Mpro enzyme.

Inhibitor	Amino acids in the binding pocket	Interaction types	No. of H-Bond
	Ser144, Cys145, Gly143	Conventional H-Bond	1, 1, 1
	His164, Asp142	Carbon H-Bond	
Co-crystalized	Met49	Pi-Sigma	
ligand	Met164	Pi-Sulfur	
	His41	Pi-Pi Stacked	
	Glu166, Gln189, Arg188, Asp187, Leu27, His163, Phe140, Leu141	Van der Waals	
	Gln189, His163	Conventional H-Bond	1,1
	His41	Pi-Pi Stacked	
Chloroquine	Met49, Met163, Cys145, Leu27	Pi-Alkyl	
	His164	Pi-Donor H-Bond	
	His172, Glu166, Asp187, Phe140, Leu141, Ser144, Asn142, Gly143, Thr25, Thr26, Val42	Van der Waals	
	Gln189, Phe140, Glu166, Cys145, Thr26	Conventional H-Bond	2,2,1,1,1
	His41	Pi-Pi Stacked	
Ritonavir	Met49, Met165, Leu27	Pi-Alkyl	
	Arg188, Ser144, Leu141, His172, Asn142, His163, Gly143, Thr25, His164, Asp187	Van der Waals	
	Cys145	Conventional H-Bond	1
Rremdesivir	Met49	Pi-Alkyl	
	His41, Thr26	Carbon H-Bond	
	His164	Unfavorable Acceptor-Acceptor	
	Asp187, Ser46, Asn142, Val42, Gln189, Leu27, Thr25, Gly143, Leu141, Ser144, His163, Phe140, Glu166, Met165	Van der Waals	
	Gln189, His163	Conventional H-Bond	1, 1
	His41	Pi-Sigma	
Gingerenone A	Met49, Met165, Cys145, Ley27	Pi-Alkyl	
	His164	Pi-Donor H-bond	
	Asp187, Phe140, Leu141, Ser144, Asn142, Gly143, Thr25, Thr26,	Van der Waals	

	Val42, His127, Glu166		
	Glu188, Phe140, Glu166, Cys141, Thr26	Conventional H-Bond	2, 2, 1, 1, 1
	Met49, Met165, Leu27	Pi-Alkyl	
Astilbin	His41	Pi-Pi Stacked	
	Ser144, Leu141, His172, Asn142, His163, Gly143, Thr25, His164, AsAsp187, Arg188	Van der Waals	
	Gln189, Glu166, Phe140, Cys145, Ser144, Leu141	Conventional H-Bond	2, 1, 1, 1, 1,1
	Met49	Pi-Alkyl	
L-(−)-catechin	His163	Pi-Pi Stacked	
	Met165, His172, Tyr118, Gly143, Asn142, His41, Seeer46	Van der Waals	

Table 4 Toxicity prediction of selected compounds and drugs by protoX-II.

Compound	Predicted LD50(mg/kg)	Hepatotoxicity	Carcinogenicity	Immunotoxicity	Mutagenicity	Cytotoxicity
Gingerenone A	2000	Inactive	Inactive	Inactive	Inactive	Inactive
Astilbin	2300	Inactive	Active	Active	Inactive	Inactive
L-(−)-Catechin	10000	Inactive	Inactive	Inactive	Inactive	Inactive
Remdesivir	1000	Inactive	Inactive	Inactive	Inactive	Inactive
Chloroquine	750	Inactive	Inactive	Active	Active	Inactive
Ritonavir	1000	Active	Inactive	Inactive	Inactive	Inactive

Table 5 Prediction of druglikness and pharmacokinetic properties of selected compounds and drugs by SwissADME online tool.

Compound	GI absorption	BBB permeant	P-gp substrate	CYP1A2 inhibitor	CYP2C19 inhibitor	CYP2C9 inhibitor	CYP2D6 inhibitor	CYP3A4 inhibitor	Lipinski's rule of five
Gingerenone A	High	Yes	No	Yes	No	Yes	Yes	Yes	Yes; 0 violation
Astilbin	Low	No	Yes	No	No	No	No	No	No; 2 violations: NorO>10, NHorOH>5
L-(−)-Catechin	High	No	Yes	No	No	No	No	No	Yes; 0 violation
Remdesivir	Low	No	No	No	No	No	No	Yes	No; 2 violations: MW>500, NorO>10
Chloroquine	High	Yes	No	Yes	No	No	Yes	Yes	Yes; 0 violation
Ritonavir	Low	No	Yes	No	No	No	No	Yes	No; 2 violations: MW>500, NorO>10

In particular, after 60 ns, the RMSD fluctuation of the L-(-)-catechin complex became more prominent, indicating substantial conformational changes and instability of this complex. Fig. 3(b) shows the root mean square fluctuations (RMSFs) of the docked and undocked Mpro proteins. Measuring the flexibility of the Cα atoms of a protein is a critical parameter in determining the stability of the proteinligand complex, which can be gauged using RMSF analysis. The RMSF values were maintained within the ranges of 0.045–0.386, 0.045–0.797, and 0.066–0.964 nm for Apo-Mpro, remdesivir, and the L-(-)-catechin complexes, respectively. The selected ligands affect and increase the flexibility of docked vise-a-vise-undocked Mpro. As for the RMSD trend, this increase was greater for the L-(−)-catechin complex throughout the simulation, especially for residues such as Glu47, Asn41, Arg76, and Gly195, and for residues 220-290. The increased fluctuations in the RMSF and RMSD of the protein complexes compared to those of Apo-Mpro could be an indication of system instability and perturbation, which may be due to conformational changes in the protein complex system and displacement of ligands inside the binding sites. Rg is the mass weight root mean square distance of the collection of atoms from their common center of mass. Thus, it provides a measure of the overall dimension and compactness of a protein. From the beginning to the end of the simulation process, the Rg of Apo-Mpro reached a plateau with minimum fluctuation. While the binding of remdesivir and L-(-)-catechin increased the value of Rg, especially after 70 ns, the Rg of the L-(−)-catechin complex became more prominent,

which indicates that it was less compact than Apo-Mpro was (Fig. 3(c).

This finding is in agreement with previous observations. Moreover, the evolution of the solvent-accessible surface area (SASA) of Apo-Mpro and the complexes was analyzed from the simulation trajectories to assess the change in Mpro volume (Fig. 3(d)). Here, similar trends were also observed for the SASA trajectories. From the beginning of the simulation, the SASA values of Apo-Mpro remained stable till the end of the simulation. However, the SASA values of the docked structures were greater than those of Apo-Mpro, indicating the expansion of the protein surface. Interestingly, similar to those of Rg and RMSD, the SASA profile of the L-(−)-catechin

complex increased significantly after 70 ns, indicating less compactness and greater mobility. This could be due to the greater binding strength of L-(−)-catechin to the binding pocket of Mpro.

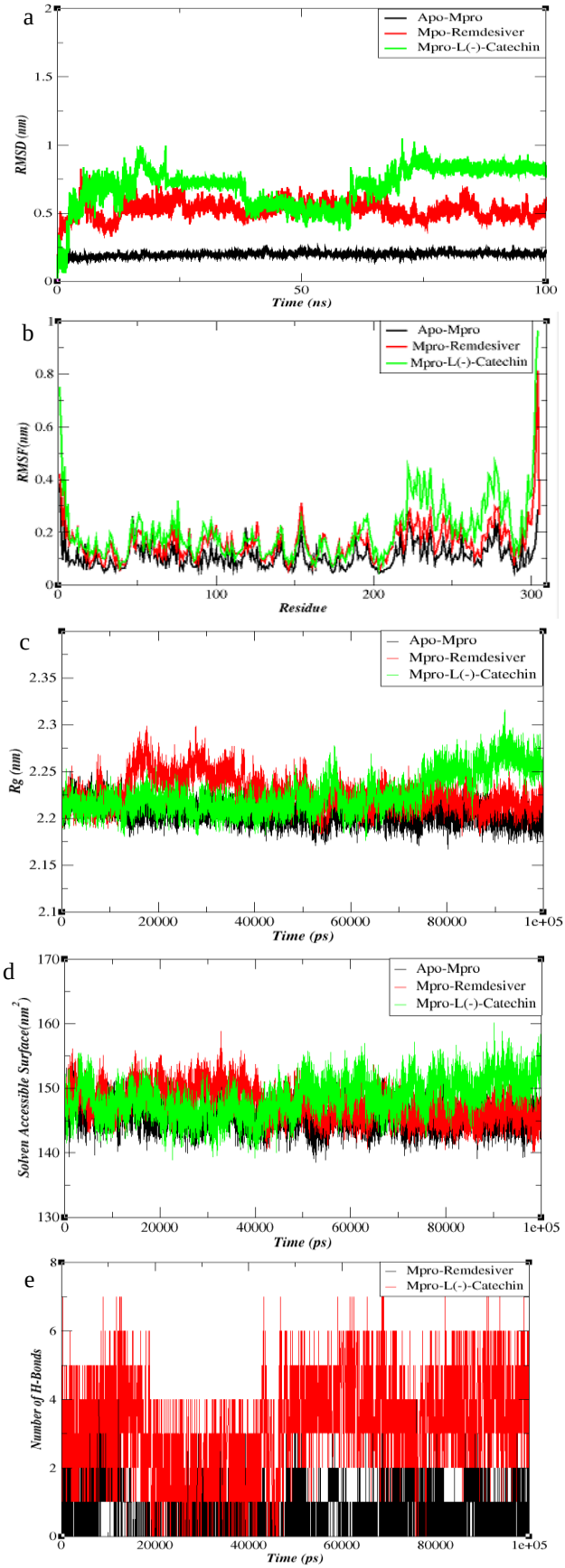

Fig. 3 (**a**) RMSD; (**b**) RMSF; (**c**) Rg; (**d**) SASA; and (**e**) Hydrogen bond profiles of the Mpro complexes during MD simulations.

An important physical parameter for molecular interactions is hydrogen bonding, which stabilizes molecular structures by minimizing the energy of systems. Based on this, we calculated the number of hydrogen bonds formed throughout the simulation for the selected complexes. Fig. 3(e) illustrates that during the equilibrium simulation, remdesivir and L-(−)-catechin had hydrogen bond ranges between 0 and 4 and between 0 and 8, with average numbers of 0.817 and 3.019, respectively. The interaction patterns revealed that the number of conformers for L-(−)-catechin complexes with more than 3 hydrogen bonds was greater than that for remdesivir. Overall, compared with those of remdesivir, MD simulation analysis revealed the formation of a favorable and stable energetic complex for L-(−)-catechin.

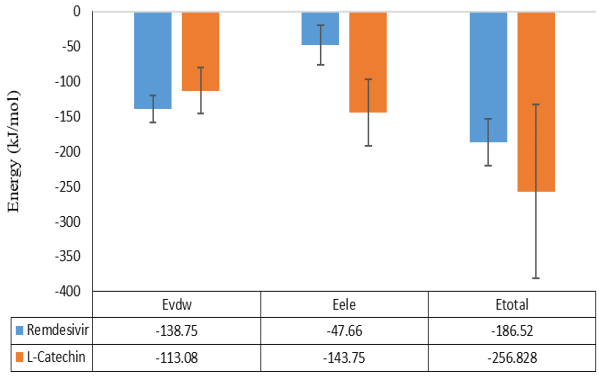

	Evdw	Eele	Etotal
Remdesivir	-138.75	-47.66	-186.52
L-Catechin	-113.08	-143.75	-256.828

Fig. 4 MM-PBSA calculations for Remdesivir and L-(−)-catechin complexes.

Interaction Analysis by MM/PBSA Binding Energy

Fig. 4, shows the van der Waals (Vdw) and electrostatic (Elec) energy shares of the total binding energy in a dynamic state, for remdesivir and L-(−)-catechin using the molecular mechanics Poisson-Boltzmann surface area (MM/PBSA) method. A greater negative binding free energy indicated a stronger interaction and increased affinity between the receptor and ligands. The most favorable binding energy was shown by L-(−)-catechin (-256.82 kJ/mol). Moreover, the decomposition of the binding energies revealed a greater contribution of the Elec energy (-143.75 kJ/mol) than the Vdw energy (-113.08 kJ/mol) to the inhibitory effect of L-(−)-catechin. The total binding energy of the Mpro complex with remdesivir was -186.52 kJ/mol. The Vdw energy contributed more favorably (-138.75 kJ/mol) than did the Elec energy (−47.66 kJ/mol). This finding is in agreement with the trajectory of the simulation time (Fig. 3(e)), in which L-(−)-catechin had a greater number of H-bonds with the Mpro protein than remdesivir at different time intervals. The estimated binding free energy of L-(−)-catechin within Mpro indicates high affinity and binding

to the active site of Mpro. This clearly shows the prominent effect of L-(−)-catechin within the Mpro cavity.

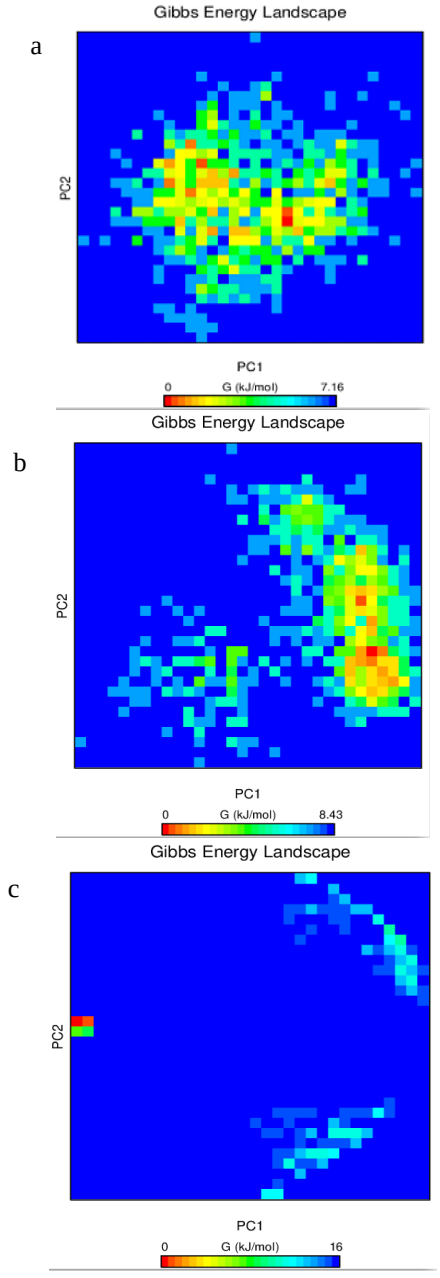

Fig. 5 The free energy landscape along the first two principal components PC1 and PC2 for (a) Apo-Mpr, (b) Remdesivir-Mpro, and (c) L-(−)-catechin-Mpro.

Free Energy Landscape (FEL)

To determine the structural properties via thermodynamic information, we constructed a free energy landscape (FEL) for the Apo-Mpro and Mpro-complexes. On the FEL, the energy minima were obtained based on the probability of a combination of MD data points to map the minimum energy configuration of the proteins. As shown in Fig. 5, the larger and more distributed red and yellow areas represent the energy minima configuration, which is clearly observed in the free energy profiles of the Apo-Mpro and remdesivir-complex, and blue shows the highest energy configuration. Additionally, the highest Gibbs energies for the Apo-Mpro and remdesivir-complex were 7.16 and 8.43 kJ/mol, respectively, while the energy was 16 kJ/mol for the L-(−)-catechin-complex, indicating that the binding of L-(−)-catechin to the Mpro protein affects the overall conformation of the system and causes it to move away from the local minimum energy state. In agreement with previous observations, i.e., RMSD, RMSF, Rg, and SASA, according to the probability energy minima distribution, the instability of the L-(−)catechin- complex was greater than that of Apo-Mpro and the remdesivir-complex.

CONCLUSION

In the present investigation, the inhibitory effects of thirteen different phytochemicals belonging to ginger and kundur with the key Mpro enzyme of SARS-CoV-2 were analyzed. The top three phytochemicals, gingerenone A, astilbin, L-(−)-catechin, and the reported antiviral agents, chloroquine, ritonavir, and remdesivir, were chosen based on their docking scores and predicted binding energies. Considering that drug-likeness and ADMET properties are important criteria during the drug development process, it was concluded that only L-(−)-catechin and remdesivir could be considered candidate molecules in the drug development processes for SARS-CoV-2 since they do not have any toxic effects or violations on eukaryotic cells. Hence, L-(−)-catechin (as a phytochemical) and remdesivir (as a reference) were selected for MD simulation studies. A molecular dynamics study showed that L-(−)-catechin greatly impact the Mpro structure. The Rg and SASA trajectories revealed that the interaction of L-(−)-catechin in the Mpro binding pocket caused more unfolding than that of remdesivir. These findings are consistent with FEL observations, that L-(−)-catechin affects the overall conformation of Mpro and destabilizes it. Furthermore, we calculated the total number of hydrogen bonds formed during the simulation time in the two complexes. The L-(-)-catechin complex formed more hydrogen bonds than did the remdesivir complex, suggesting that the interaction of L-(−)-catechin in the binding pocket of Mpro of SARS-CoV-2 was greater than that of the remdesivir complex. These results were further evaluated and confirmed by MM/PBSA binding free energy calculations. L-(−)-catechin had a greater binding energy than remdesivir. H-bonds and electrostatic interactions facilitate binding between L-(-)-catechin in the Mpro binding pocket. Hence, this study reports that L-(−)-catechin is a more potent Mpro inhibitor of SARS-CoV-2. L-(−)-catechin is a polyphenol called the flavonoid present in kundur. The inhibitory potential of the purified compound against Mpro of SARS-CoV 2 could be tested using various in-vitro and in-vivo studies. In addition, the backbone structure of L-(−)-catechin can be further exploited to develop more potent SARS-CoV-2 Mpro inhibitors. Given that no treatment for coronavirus

infection has been developed thus far, these data could help to identify L-(−)-catechin or its derivatives for the treatment of COVID-19 after a clinical trial. We hope that the results of this study will provide insight for upcoming academicians in anti-SARS-CoV-2 research.

Acknowledgements

This study was financially supported by Islamic Azad University of Gorgan.

Data Availability Statement

Most data generated or analysed during this study are included in this article. All data will be available upon request of the reviewer or journal editorial board.

Conflict of Interest

On behalf of all authors, the corresponding author states that there is no conflict of interest.

REFERENCES

1. Gorbalenya A.E., Baker S.C., Baric R.S., de Groot R.J., Drosten C., Gulyaeva A.A., Haagmans B.L., Lauber C., Leontovich A.M., Neuman B.W., Penzar D., Perlman S., Poon L.L.M., Samborskiy D. V., Sidorov I. A., Sola I., Ziebuhr J. The species Severe acute respiratory syndrome-related coronavirus: classifying 2019-nCoV and naming it SARS-CoV-2. Nat Microbiol. 2020;5(4):536–544.
2. Krammer F. SARS-CoV-2 vaccines in development. Nature 2020;586(7830):516–527.
3. Wardeh M., Baylis M., Blagrove M.S.C. Predicting mammalian hosts in which novel coronaviruses can be generated. Nat Communs. 2021;12(1):780.
4. Ahmad S., Usman Mirza M., Yean Kee L., Nazir M., Abdul Rahman N., Trant J. F., Abdullah I. Fragment-based in silico design of SARS-CoV-2 main protease inhibitors. Chem Biol Drug Design 2021;98(4):604-619.
5. Zhang L., Lin D., Sun X., Curth U., Drosten C., Sauerhering L., Becker S., Rox K., Hilgenfeld R. Crystal structure of SARS-CoV-2 main protease provides a basis for design of improved a-ketoamide inhibitors. Science 2020;368(6489):409–412.
6. Hilgenfeld R. From SARS to MERS: crystallographic studies on coronaviral proteases enable antiviral drug design. The FEBS J. 2014;281(18):4085–4096.
7. Jia Z., Lan X., Lu K., Meng X., Jing W., Jia S., Zhao K., Dai Y. Synthesis, molecular docking, and binding Gibbs free energy calculation of -nitrostyrene derivatives: Potential inhibitors of SARS-CoV-2 3CL protease. J Molecul Struct. 2023;1284:135409.
8. Mandal A., Jha A.K., Hazra B. Plant Products as Inhibitors of Coronavirus 3CL Protease. Front Pharmacol. 2021;12(4):1–16.
9. Jin Z., Du X., Xu Y., Deng Y., Liu M., Zhao Y., Zhang B., Li X., Zhang L., Peng C., Duan Y., Yu J., Wang L., Yang K., Liu F., Jiang R., Yang X., You T., Liu X., *et al*. Structure of Mpro from SARS-CoV-2 and discovery of its inhibitors. Nature 2020;582(7811):289–293.
10. Citarella A., Scala A., Piperno A., Micale N. Sars-cov-2 mpro: A potential target for peptidomimetics and small-molecule inhibitors. Biomolecules 2021;11(4):607.
11. Ramajayam R., Tan K.-P., Liang P.-H. Recent development of 3C and 3CL protease inhibitors for anti-coronavirus and anti-picornavirus drug discovery. Biochem Soci Transact. 2011;39(5):1371–1375.
12. Dong L., Hu S., Gao J. Discovering drugs to treat coronavirus disease 2019 (COVID-19). Drug Discover Therapeut. 2020;14(1):58–60.
13. Kumar D.C.V., Chethan B.S., Shalini V., Rangappa K.S., Lokanath N.K. Structural elucidation and in-silico evaluation of 1, 2, 4-triazole derivative as potent Omicron variant of SARS-CoV-2 spike protein inhibitor with pharmacokinetics ADMET and drug-likeness predictions. J Mol Struct. 2024;12(97):136976.
14. Ni L., Zhou L., Zhou M., Zhao J., Wang D.W. Combination of western medicine and Chinese traditional patent medicine in treating a family case of COVID-19. Front Med. 2020;14(2):210–214.
15. Wang M., Cao R., Zhang L., Yang X., Liu J., Xu M., Shi Z., Hu Z., Zhong W., Xiao G. Remdesivir and chloroquine effectively inhibit the recently emerged novel coronavirus (2019-nCoV) in vitro. Cell Res. 2020;30(3):269–271.
16. Mirza M.U., Froeyen M. Structural elucidation of SARS-CoV-2 vital proteins: Computational methods reveal potential drug candidates against main protease, Nsp12 polymerase and Nsp13 helicase. J Pharmaceut Anal. 2020;10(4):320–328.
17. Bellanger R.A., Seeger C.M., Smith H.E. Safety of complementary and alternative medicine (CAM) treatments and practices. Side Eff Drugs Annu. 2018;40:609–619.
18. Jahan R., Paul A. K., Bondhon T. A., Hasan A., Jannat K., Mahboob T., Nissapatorn V., Pereira M. de L., Wiart C., Wilairatana P., Rahmatullah, M. *Zingiber officinale*: Ayurvedic Uses of the Plant and In Silico Binding Studies of Selected Phytochemicals With Mpro of SARS-CoV-2. Nat Prod Commun. 2021;16(10).
19. Ayub M.A., Hanif M.A., Sarfraz R.A., Shahid M. Biological activity of *Boswellia serrata* roxb. Oleo gum resin essential oil: Effects of extraction by supercritical carbon dioxide and traditional methods. Int J Food Prop. 2018;21(1):808–820.
20. Roy N.K., Parama D., Banik K., Bordoloi D., Devi A.K., Thakur K.K., Padmavathi G., Shakibaei M., Fan L., Sethi G., Kunnumakkara A. B. An update on pharmacological potential of boswellic acids against chronic diseases. Int J Mol Sci. 2019;20(17).
21. Sultana A., Raheman K. Boswellia serrata Roxb. a traditional herb with versatile pharmacological activity: a review. Int J Pharmaceut Sci Res. 2013;4(6):2106-2117.
22. Wang J., Prinz R.A., Liu X., Xu X. In vitro and in vivo antiviral activity of gingerenone a on influenza a virus is mediated by targeting janus kinase 2. Viruses 2020;12(10):1–18.
23. Abd El-Wahab A., El-Adawi H., El-Demellawy M. In vitro study of the antiviral activity of *Zingiber officinale*. Planta Medica 2009; 75(09)-PF7.
24. Rahmani A.H., Al Shabrmi F.M., Aly S.M. Active ingredients of ginger as potential candidates in the prevention and treatment of diseases via modulation of biological activities. Int J Physiol Pathophysiol Pharmacol. 2014;6(2):125–136.
25. Zaini N.A.M., Anwar F., Hamid A.A., Saari N. Kundur [*Benincasa hispida* (Thunb.) Cogn.]: A potential source for valuable nutrients and functional foods. Food Res Int. 2011;44(7):2368–2376.
26. O'Boyle N.M., Banck M., James C.A., Morley C., Vandermeersch T., Hutchison G. R. Open Babel: An Open chemical toolbox. J Cheminf. 2011;3(10):33.
27. Pettersen E.F., Goddard T.D., Huang C.C., Couch G.S., Greenblatt D.M., Meng E.C., Ferrin T.E. UCSF Chimera - A

visualization system for exploratory research and analysis. J Comput Chem. 2004;25(13):1605–1612.
28. Goodsell D.S. Computational docking of biomolecular complexes with autodock. Cold Spring Harbor Protocols. 2009; 4(5). https://doi.org/10.1101/pdb.prot5200
29. Abraham M.J., Murtola T., Schulz R., Páll S., Smith J.C., Hess B., Lindah E. Gromacs: High performance molecular simulations through multi-level parallelism from laptops to supercomputers. SoftwareX. 2015;1(2):19–25.
30. Hess B., Kutzner C., Van Der Spoel D., Lindahl E. GRGMACS 4: Algorithms for highly efficient, load-balanced, and scalable molecular simulation. J Chem Theor Comput. 2008;4(3):435–447.
31. Van Der Spoel D., Lindahl E., Hess B., Groenhof G., Mark AE., Berendsen HJC. GROMACS: Fast, flexible, and free. J Comput Chem. 2005;26(16):1701–1718. https://doi.org/10.1002/jcc.20291
32. Schüttelkopf A.W., Van Aalten D.M.F. PRODRG: A tool for high-throughput crystallography of protein-ligand complexes. Acta Crystallographica Sect D: Biol Crystallograph. 2004;60(8):1355–1363.
33. Darden T., York D., Pedersen L. Particle mesh Ewald: An N·log(N) method for Ewald sums in large systems. J Cheml Physics 1993;98(12):10089–10092.
34. Homeyer N., Gohlke H. Free energy calculations by the Molecular Mechanics Poisson-Boltzmann Surface Area method. Mol Inform. 2012;31(2):114–122.
35. Aier I., Varadwaj P. K., Raj U. Structural insights into conformational stability of both wild-type and mutant EZH2 receptor. Sci Rep. 2016;6(7):1–10.
36. Gaur R., Thakur J.P., Yadav D.K., Kapkoti D.S., Verma R.K., Gupta N., Khan F., Saikia D., Bhakuni R.S. Synthesis, antitubercular activity, and molecular modeling studies of analogues of isoliquiritigenin and liquiritigenin, bioactive components from *Glycyrrhiza glabra*. Med Chem Res. 2015;24(9):3494–3503.
37. Ponnan P., Gupta S., Chopra M., Tandon R., Baghel A.S., Gupta G., Prasad A.K., Rastogi R.C., Bose M., Raj H.G. 2D-QSAR, Docking Studies, and In Silico ADMET Prediction of Polyphenolic Acetates as Substrates for Protein Acetyltransferase Function of Glutamine Synthetase of Mycobacterium tuberculosis . ISRN Struct Biol. 2013;(11):1–12.
38. Mahase E. Covid-19: US approves remdesivir despite WHO trial showing lack of efficacy. British Med J Publishing Group. 2020;371:m4120.
39. Halsey G, Remdesivir Gets FDA" OK" for COVID-19 Treatment in Hepatic Disease Across Stages. Patient Care (Online). 2023.
40. Garibaldi B.T., Wang K., Robinson M.L., Zeger S.L., Bandeen-Roche K., Wang M.C., Alexander G.C., Gupta A., Bollinger R., Xu Y. Comparison of time to clinical improvement with vs without remdesivir treatment in hospitalized patients with COVID-19. JAMA Network Open 2021;4(3):e213071.
41. Singh R., Bhardwaj V.K., Das P., Purohit R. A computational approach for rational discovery of inhibitors for non-structural protein 1 of SARS-CoV-2. Comput Biol Med. 2021;135:104555.